Journal of Solid State Chemistry **164,** 292–300 (2002)
doi:10.1006/jssc.2001.9474, available online at http://www/idealibrary.com on IDEAL®

Magnetic and Transport Properties of $RESn_xSb_2$ (RE = La, Ce, Pr, Nd, Sm; x = 0.5, 0.7)

Laura Deakin, Michael J. Ferguson, Michael J. Sprague, and Arthur Mar[1]

Department of Chemistry, University of Alberta, Edmonton, Alberta, Canada T6G 2G2

and

R. D. Sharma and Colin H. W. Jones

Department of Chemistry, Simon Fraser University, Burnaby, British Columbia, Canada V5A 1S6

Received July 31, 2001; in revised form November 5, 2001; accepted November 18, 2001; published online February 11, 2001

The nonstoichiometric rare-earth tin antimonides $RESn_xSb_2$ (RE = La, Ce, Pr, Nd, Sm) were characterized by ^{119}Sn Mössbauer spectroscopy and their transport and magnetic properties were measured. The presence of nearly zero-valent Sn is suggested by the similarity of the ^{119}Sn Mössbauer parameters in $LaSn_xSb_2$ ($0.1 \le x \le 0.7$) to those of elemental β-Sn. All $RESn_{0.7}Sb_2$ compounds exhibit metallic behavior. $CeSn_{0.7}Sb_2$ and $NdSn_{0.7}Sb_2$ show drops in resistivity below 8 K; this is attributed to a transition to a magnetically ordered state. At 25 K, $CeSn_{0.7}Sb_2$ also displays a resistivity minimum characteristic of ordered Kondo lattices. Magnetic studies indicate that, below 4 K, $CeSn_xSb_2$ ($x = 0.5, 0.7$) orders ferromagnetically, whereas $NdSn_xSb_2$ ($x = 0.5, 0.7$) orders antiferromagnetically and undergoes a metamagnetic transition at $H_C = 5.5$ T and 2 K. Neither $PrSn_xSb_2$ nor $SmSn_xSb_2$ ($x = 0.5$, 0.7) displays long-range magnetic ordering above 2 K.

Key Words: **antimonide; Mössbauer spectroscopy; magnetic properties; transport properties.**

INTRODUCTION

Nonstoichiometry is sometimes viewed as a nuisance in the characterization of solid state compounds, but it provides an opportunity to study how properties change as a function of composition and structure. In the series of nonstoichiometric ternary rare-earth tin antimonides $RESn_xSb_2$, not only can the amount of Sn be varied over a wide range ($0.1 \le x \le 0.7$), but rare-earth substitutions (RE = La–Nd, Sm) can also impart changes in the electronic structures (1). On the basis of the single-crystal structure determination of $LaSn_{0.75}Sb_2$ (1), the structure of $RESn_xSb_2$ can be built up by inserting Sn atoms, which partially occupy disordered sites arranged in linear chains, into the structure of the binary rare-earth diantimonides $RESb_2$ (2, 3), which in turn consists of square sheets of Sb atoms and layers of Sb_2 pairs separated by the RE ions (Fig. 1). In a formal sense, neutral Sn chains are inserted between layers of composition $RESb_2$: $^2_\infty[RESb_2] + x\,^1_\infty[Sn] = {}^3_\infty[RESn_xSb_2]$. Increasing the Sn content from $x = 0.1$ to $x = 0.7$ does not significantly alter interlayer separations (as gauged by the b parameter), but leads to distortions of the $RESb_2$ layer as manifested by a decrease in the a and an increase in the c parameter.

The binary rare-earth diantimonides $RESb_2$ themselves display a wide range of behaviors, such as superconductivity in $LaSb_2$ (4), antiferromagnetism in $CeSb_2$ (5), although previously this was suggested to be a ferromagnet (6), metamagnetism in $PrSb_2$ (7) and $NdSb_2$ (5), and antiferromagnetism and high magnetoresistance in $SmSb_2$ (6). These diantimonides are already highly anisotropic in their properties. The insertion of Sn chains between $^2_\infty[RESb_2]$ layers would be expected to enhance the anisotropy even further. With the magnetic properties originating exclusively from the RE ions, prying the $^2_\infty[RESb_2]$ layers further apart will diminish coupling interactions. Figure 2, which shows the structures of $LaSb_2$ and $LaSn_{0.75}Sb_2$ with all metalloid (Sn, Sb) atoms omitted, reveals the dramatic increase in the interlayer separation between RE ions upon insertion of the Sn chains.

To probe the electronic environment of the Sn atoms in the disordered chains, a ^{119}Sn Mössbauer study was carried out on the nonmagnetic $LaSn_xSb_2$ ($0.1 \le x \le 0.7$) series. The

[1]To whom correspondence should be addressed. Fax: (780) 492-8231. E-mail: arthur.mar@ualberta.ca.

0022-4596/02 $35.00

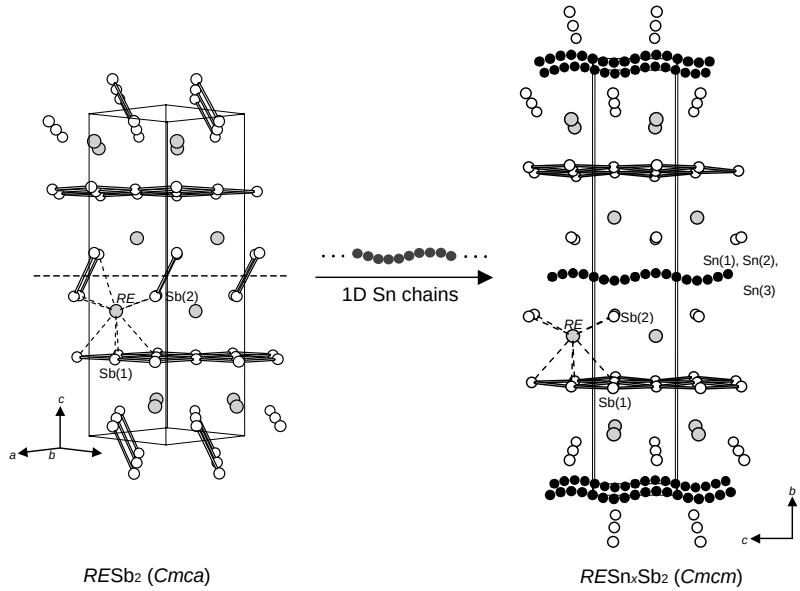

FIG. 1. Structure of $RESn_xSb_2$ as a composite of $RESb_2$ (RE = La–Nd, Sm) and 1D Sn chains.

transport and magnetic properties of $RESn_{0.5}Sb_2$ and $RESn_{0.7}Sb_2$ (RE = La–Nd, Sm) were then determined to draw comparisons to the parent $RESb_2$ compounds.

EXPERIMENTAL

Synthesis

Bulk-phase samples of $RESn_xSb_2$ ($0.1 \leq x \leq 0.7$ for RE = La; $x = 0.5$, 0.7 for RE = Ce, Pr, Nd, Sm) were prepared from reactions of powders of the elements (La, Ce, Pr, Nd, 99.9%, Alfa-Aesar; Sm, 99.9%, Aldrich; Sn, 99.8%, Cerac; Sb, 99.995%, Aldrich). Stoichiometric mixtures of the elements were loaded into fused-silica tubes (5-cm length, 10-mm i.d.), which were then evacuated, sealed, and heated at 570°C for 1 day and 950°C for 2 days, cooled to 500°C over 1 day, and then cooled to room temperature over 12 h. The products were analyzed by powder X-ray diffraction patterns collected on an Enraf-Nonius FR552 Guinier camera ($CuK\alpha_1$ radiation; Si standard). For all $LaSn_xSb_2$ reactions with $x \leq 0.7$, the ternary compounds were the only identifiable products.

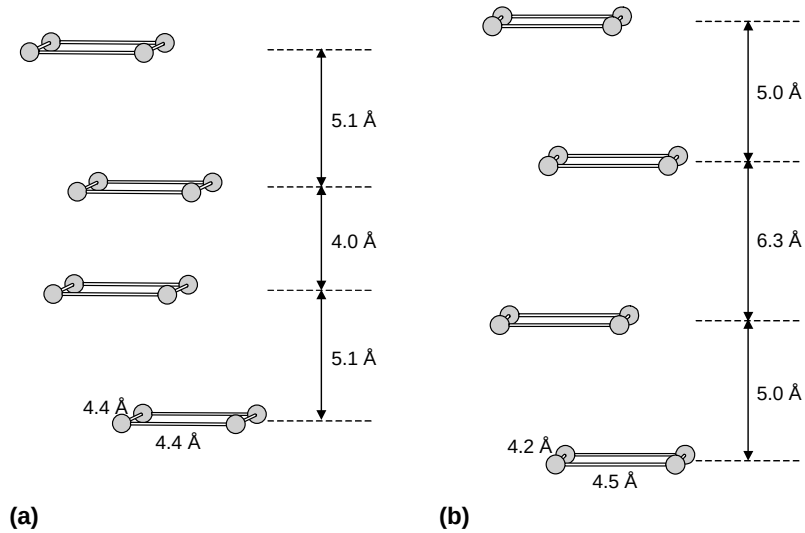

FIG. 2. Structures of (a) $LaSb_2$ and (b) $LaSn_{0.75}Sb_2$, with the metalloid (Sn, Sb) atoms omitted. The sheets of La atoms are spread further apart upon insertion of Sn chains upon going from $LaSb_2$ to $LaSn_{0.75}Sb_2$.

Pure ternary compounds could not be synthesized for $RESn_xSb_2$ with RE = Ce, Pr, Nd, Sm and $x < 0.5$ as these samples showed the presence of binary antimonide impurities.

Structure Determination of $LaSn_{0.5}Sb_2$

It was of interest to determine the structure of a $LaSn_xSb_2$ member possessing less than the maximum possible Sn content, for the purpose of comparison to the $LaSn_{0.75}Sb_2$ structure and for complementing the ^{119}Sn Mössbauer data. Crystals from the nominal reaction "$LaSn_{0.5}Sb_2$" were selected and mounted for EDX (energy-dispersive X-ray) analysis on a Hitachi S-2700 scanning electron microscope. Anal. (mol %) Calcd for $LaSn_{0.5}Sb_2$: La, 28.6%; Sn, 14.3%; Sb, 57.1%. Found (average of five analyses): La, 29.0(5)%; Sn, 13.9(5)%; Sb, 57.1(6)%. Details of the structure determination, in the form of a CIF, have been sent to Fachinformationszentrum Karlsruhe, Abt. PROKA, 76344 Eggenstein-Leopoldshafen, Germany, as supplementary material No. CSD-412231 and can be obtained by contacting FIZ (quoting the article details and the corresponding CSD numbers). Refinement of the diffraction data converged to residuals of $R_w(F_o^2)$ of 0.148 and $R(F)$ (for $F_o^2 > 2\sigma(F_o^2)$) of 0.047 and led to a formula of $LaSn_{0.53(1)}Sb_2$. $LaSn_{0.5}Sb_2$ is isostructural to $LaSn_{0.75}Sb_2$; in particular, the disordered Sn atoms are located in the same three sites in the structure, with reduced partial occupancy in each but with no pronounced preferences in the site occupation.

Mössbauer Spectroscopy

^{119}Sn Mössbauer spectra for the series $LaSn_xSb_2$ ($0.1 \le x \le 0.7$) were recorded with use of a Harwell Instruments MWG 200 constant acceleration drive, equipped with an MSA 200 attenuator, and a NaI scintillation counter. An Amersham 5-mCi $CaSnO_3$ source was used. The absorbers were immersed in liquid nitrogen. Reference spectra were routinely measured for β-Sn and SnO_2. Isomer shifts are reported with respect to SnO_2 at 77 K. The spectrometer was calibrated regularly using an ^{57}Co/Rh source (10 mCi; Amersham) and an iron foil at room temperature.

Transport and Magnetic Measurements

Electrical resistivities were measured by standard four-probe techniques on a Quantum Design PPMS system equipped with an ac-transport controller (Model 7100). The current was 100 μA and the frequency was 16 Hz. The resistivity was measured along the needle axis (crystallographic a axis) of single crystals of $LaSn_{0.7}Sb_2$, $PrSn_{0.7}Sb_2$, and $SmSn_{0.7}Sb_2$. For $CeSn_{0.7}Sb_2$ and $NdSn_{0.7}Sb_2$, polycrystalline samples were used, owing to unavailability of suitably sized crystals.

Magnetic measurements for powder samples of $RESn_xSb_2$ were made on a Quantum Design PPMS 9 T magnetometer/susceptometer between 2 and 300 K and in applied fields up to 9 T. Magnetization data as a function of temperature were collected under zero-field-cooled conditions upon warming in an applied field of 0.1 T, except for RE = Sm where $H = 0.5$ T. Magnetic ordering temperatures were determined from ac magnetic susceptibility measurements, which were made with a driving amplitude of 1.0 Oe and a frequency of 1000 Hz. All magnetic data were corrected for holder and sample diamagnetism.

RESULTS AND DISCUSSION

Sn Sites in $LaSn_xSb_2$

In the $RESn_xSb_2$ (RE = La–Nd, Sm) series, the orthorhombic structure of $LaSn_{0.75}Sb_2$ (*Cmcm*) has been previously determined (1). Its distinguishing feature is the presence of chains containing three types of sites, closely spaced at increments of ~0.5–0.6 Å, which are partially occupied by Sn. The maximum occupancy in each site is ~20%, consistent with a local distribution of Sn atoms occupying every fifth site so that they are spaced at least ~2.8 Å apart, which corresponds to a reasonable Sn–Sn bonding distance. The structure of $LaSn_{0.5}Sb_2$, which has less than the maximum possible Sn content, has been shown to be essentially identical to that of $LaSn_{0.75}Sb_2$, but with reduced occupancies of ~13% in each of the three Sn sites. Two interpretations for a local model can be envisioned: (i) Every seventh (or eighth) site is occupied, resulting in Sn–Sn distances of ~3.9 Å that are too long to be bonding (Fig. 3a), or (ii) every fifth site is occupied to form ~2.8 Å Sn–Sn bonds, but the chains are randomly segmented by vacancies such that, on average, only one in seven (or eight) sites is occupied (Fig. 3b). We favor the second interpretation because it retains strong Sn–Sn bonds, which are likely an integral part of the structure, and we assume that all members in the $RESn_xSb_2$ series adopt this structure.

The nature of the Sn atoms in these chains has been a long-standing question. On the basis of now well-established electron-counting rules for structures containing Sb networks (8), the isolated Sb atoms are assigned an oxidation state of −3 and those in the square nets with long, ~3.0 Å (approximately half bond order), Sb–Sb bonds are assigned an oxidation state of −1. For $LaSn_{0.5}Sb_2$, for instance, the formulation $(La^{3+})(Sn^{2+})_{0.5}(Sb(1)^{1-})(Sb(2)^{3-})$ can be proposed. This approach implies that as the Sn content, x, decreases in $LaSn_xSb_2$, the oxidation state of the Sn atoms increases, eventually to

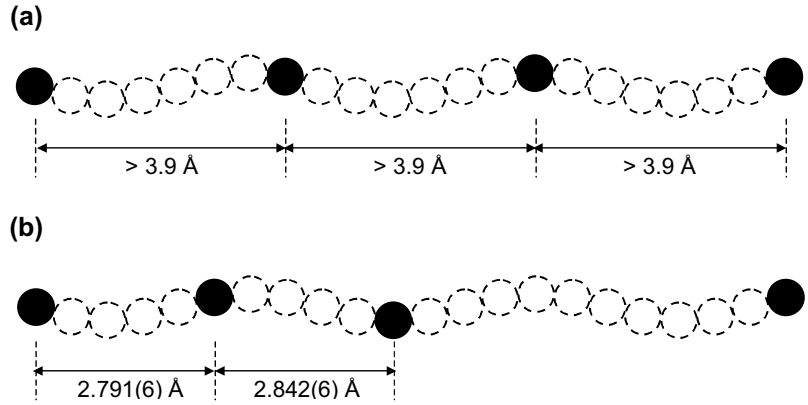

FIG. 3. Two possible arrangements of the Sn atoms in $LaSn_{0.5}Sb_2$, with $\sim 13\%$ occupancy of the Sn sites. (a) One in *seven* Sn sites occupied, with Sn–Sn distances greater than 3.9 Å and outside the realm of bonding. (b) One in *five* sites occupied on a local level, with reasonable Sn–Sn bonding distances. The effect of reducing the Sn content from its maximum of $x = 0.75$ is the creation of vacancies and the segmentation of the infinite Sn chains into finite units.

unrealistic values. Alternatively, an Sb square net has been shown to be capable of serving as an electron source or sink, releasing or absorbing electrons as needed (8–10), so the Sb(1) oxidation state may vary. Given that the electronegativities of Sn (1.96) and Sb (2.05) are similar, the Sn–Sb(2) bonds will in fact be strongly covalent; therefore, an oxidation state formalism that assumes a highly polar Sn–Sb bond gives a poor approximation to the true charges.

^{119}Sn Mössbauer spectroscopy was performed on the series $LaSn_xSb_2$ ($0.1 \leq x \leq 0.7$) to probe the electronic environment of the Sn atoms as a function of Sn content. For all compounds, the spectra could be fitted to a pair of overlapping Lorentzian functions constrained to have equal linewidths for any one compound, and with linewidths in the range of 1.01 to 1.31 mm s^{-1}. The spectra are consistent with the presence of a quadrupole split doublet with isomer shifts δ relative to SnO_2 of 2.58 to 2.81 mm s^{-1} and quadrupole splittings Δ of 0.97 to 1.14 mm s^{-1} (Fig. 4). It may be concluded that, in each compound, the three inequivalent Sn atoms all have very similar Mössbauer parameters, each with an isomer shift comparable to that of elemental β-Sn (2.52 mm s^{-1}) (11) and each exhibiting comparable, small quadrupole splittings. A small asymmetry in the intensity between the two fitted lines in each spectrum suggests that the Mössbauer parameters for the three types of Sn atoms in each compound, while very similar, are not exactly the same; however, the small differences were not resolvable.

The similarity of the Mössbauer parameters for $LaSn_xSb_2$ to elemental β-Sn supports the proposition that the Sn chains in $LaSn_xSb_2$ are composed of essentially zero-valent tin. The values of the isomer shifts and the quadrupole splittings are consistent with covalency between Sn atoms in the chains and between the atoms in

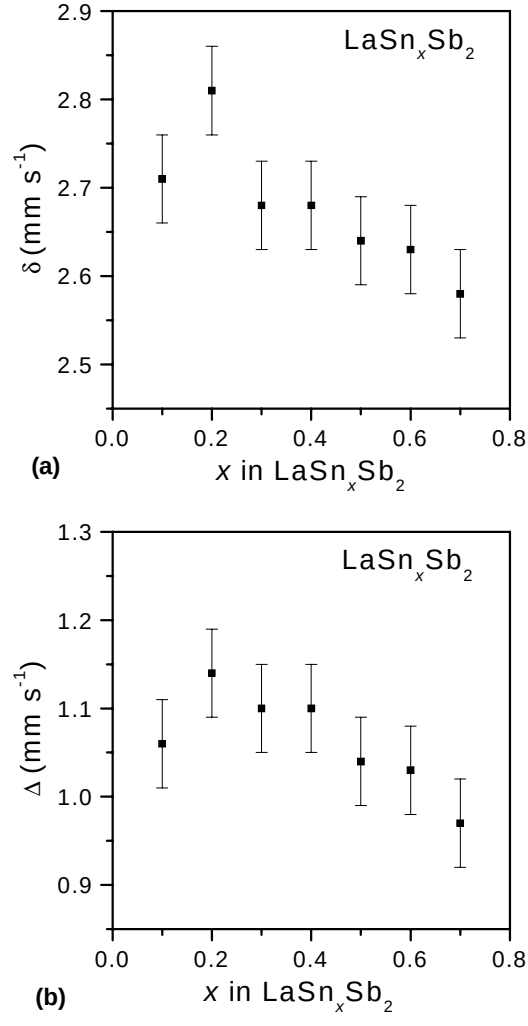

FIG. 4. ^{119}Sn Mössbauer parameters in $LaSn_xSb_2$: (a) isomer shift (δ) relative to SnO_2 and (b) quadrupole splitting (Δ) plotted as a function of Sn content, x. Note that β-Sn has an isomer shift of 2.52 mm s^{-1}.

these chains and the Sb(2) atoms; little electron transfer takes place. The small increase in isomer shift with decreasing x is indicative of partial oxidation of the Sn atoms and reflects the subtle changes that occur to accommodate the varying electron count with changing stoichiometry.

The simple model of the electronic structure based on oxidation states is inconsistent with the Mössbauer results as it assumes full electron transfer from Sn to Sb. A more accurate model based on formal charges would have to take into account that the Sn atoms are covalently bonded to the neighboring Sb(2) atoms. On average, because each Sn atom is four-bonded (to two other Sn atoms and two Sb(2) atoms) and each Sb(2) atom is bonded to one Sn atom, they are assigned as Sn^0 and $Sb(2)^{2-}$, respectively. To a first approximation, the formulation $(La^{3+})(Sn^0)_x(Sb(1)^{1-})(Sb(2)^{2-})$ is able to account for the variable Sn content. However, lowering the Sn content not only introduces vacancies along the Sn chains, thereby eliminating Sn–Sn bonds, but also eliminates some Sn–Sb(2) bonds. Further modification of this scheme is necessary and is most easily accommodated by invoking electron count fluctuations in the Sb(1) square nets.

Transport and Magnetic Properties of $RESn_xSb_2$

Metallic, or semimetallic, behavior is indicated by the general increase in electrical resistivities of $RESn_{0.7}Sb_2$ (RE = La–Nd, Sm) with increasing temperature, as shown in Fig. 5, but there are some prominent transitions in the case of $LaSn_{0.7}Sb_2$, $CeSn_{0.7}Sb_2$, and $NdSn_{0.7}Sb_2$. Magnetic data for $RESn_xSb_2$ (RE = Ce, Pr, Nd, Sm; $x = 0.5, 0.7$) are summarized in Table 1.

$LaSn_xSb_2$. The resistivity of $LaSn_{0.75}Sb_2$ was previously measured down only to 20 K (1). The resistivity has now been measured down to 2 K; it begins to drop at temperatures just above 2 K (Fig. 5a). Although resistivity measurements below 2 K could not be undertaken, it is possible that $LaSn_{0.7}Sb_2$, like the binary compound $LaSb_2$, becomes a superconductor at very low temperatures; $LaSb_2$ undergoes a transition to the superconducting state at 0.4 K (4).

Under high fields (2 T), $LaSn_{0.7}Sb_2$ displays essentially temperature-independent magnetic susceptibility ($M/H = 3.2 \times 10^{-4}$ emu/f.u.) arising from Pauli paramagnetism with a weak Curie tail at low temperatures attributable to a minor paramagnetic impurity (Fig. 6). Unfortunately, the negative χ'_{ac} magnetic susceptibility signal between 2 and 3 K was too weak to clearly observe the Meissner effect. The transition in the resistivity at high temperatures, $T = \sim 250$ K, is reminiscent of the resistivity maximum seen upon formation of a charge density wave (CDW) and was found to be reproducible. The crystallographic cell parameters were determined at temperatures above and below 250 K by single-crystal X-ray diffraction in an effort to observe the periodic lattice distortions associated with a CDW state; no cell changes were observed. While this lattice distortion and CDW state would suppress superconductivity, these phenomena are known to coexist (12). The absence of a change in the magnetic susceptibility at

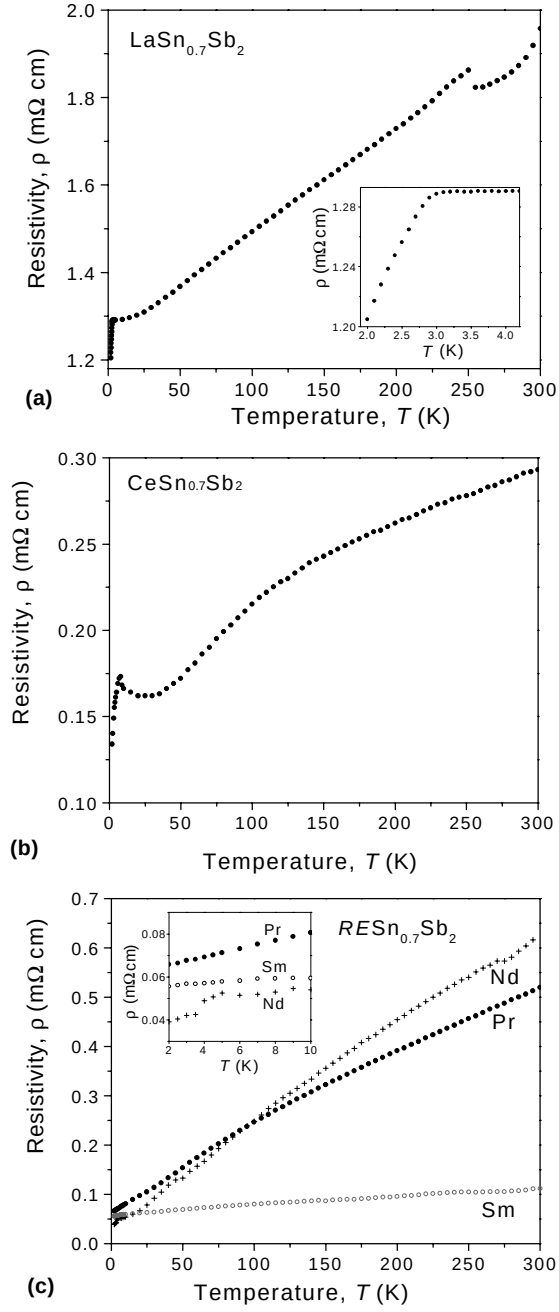

FIG. 5. Zero-field electrical resistivity between 2 and 300 K for (a) $LaSn_{0.7}Sb_2$, (b) $CeSn_{0.7}Sb_2$, and (c) $RESn_{0.7}Sb_2$ (RE = Pr, Nd, Sm). Insets display low-temperature behavior.

TABLE 1
Magnetic Data for $RESn_xSb_2$ (RE = Ce, Pr, Nd, Sm; x = 0.5, 0.7)

Compound	μ_{eff}(300 K) (μ_B)	θ (K)	M_{sat} (μ_B)	H_C (T)	T_C or T_N (K)
$CeSn_{0.5}Sb_2$	2.61	−140	1.46		3.20
$CeSn_{0.7}Sb_2$	2.69	−125	1.35		3.50
$PrSn_{0.5}Sb_2$	3.52	−27			
$PrSn_{0.7}Sb_2$	3.73	−26			
$NdSn_{0.5}Sb_2$	3.17	−14		5.37	4.0
$NdSn_{0.7}Sb_2$	3.36	−28		5.56	3.8
$SmSn_{0.5}Sb_2$	1.51				
$SmSn_{0.7}Sb_2$	1.57				

250 K may be the result of impurity paramagnetic phases present in the powder sample.

$CeSn_xSb_2$. The temperature dependence of the resistivity of a polycrystalline sample of $CeSn_{0.7}Sb_2$ (Fig. 5b) is reminiscent of the behavior of magnetically ordered Kondo lattices—the resistivity shows a local minimum at ~25 K and then undergoes a drop at lower temperatures as a result of long-range magnetic ordering. It remains to be seen whether this Kondo-like behavior is observed in single-crystal measurements; unfortunately, suitably sized crystals were unavailable.

Figure 7a shows the temperature dependence of the inverse magnetic susceptibility (H/M) for $CeSn_{0.7}Sb_2$ and $CeSn_{0.5}Sb_2$. A fit of the magnetic susceptibility above 150 K to the equation $\chi = C/(T-\theta)$ leads to negative θ values of −125 K for $CeSn_{0.7}Sb_2$ and −140 K for $CeSn_{0.5}Sb_2$, suggesting that the dominant interaction between Ce ions is antiferromagnetic, although magnetocrystalline anisotropy and Ce ion valence fluctuations may also be contributing factors. Although single-crystal anisotropic magnetization studies could not be performed for the $CeSn_xSb_2$ series, there is an interesting correspondence in their behaviour with that of $CeSb_2$, for which $\theta = -170$ K is perpendicular to the planes of Sb square nets whereas $\theta = 26$ K is observed parallel to these planes (5). This leads to an antiferromagnetic state, one of several magnetic phases present for $CeSb_2$, whereas the low-temperature magnetic behavior for $CeSn_xSb_2$ is consistent with a ferromagnetic ground state.

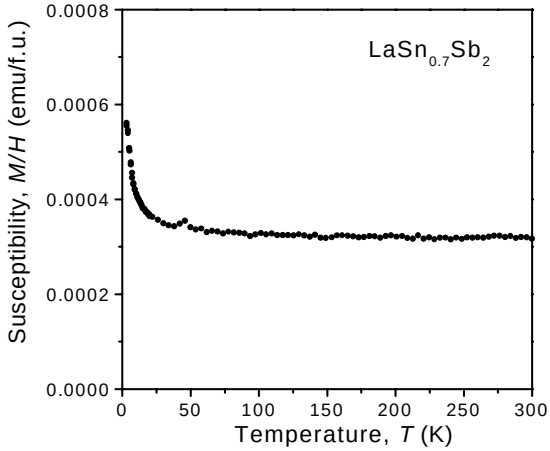

FIG. 6. Magnetic susceptibility (M/H) of $LaSn_{0.7}Sb_2$ under 2-T field. The peak near 50 K is attributed to oxygen contamination.

The effective moment at 300 K of 2.6 μ_B/Ce in $CeSn_xSb_2$ is close to that for $CeSb_2$ (2.63 μ_B/Ce) (5). However, it has been suggested that $CeSb_2$ may have an intermediate valence between +3 and +4 at low temperatures (5), and this may equally be the case for $CeSn_xSb_2$. Electronic structure calculations and electronic spectroscopy experiments for both $CeSn_xSb_2$ and $CeSb_2$ are required to understand their low-temperature behavior further.

Ferromagnetism below a T_C of 3.5 K in $CeSn_{0.7}Sb_2$ and 3.2 K in $CeSn_{0.5}Sb_2$ is supported by the presence of maxima in the real (χ'_{ac}) (inset of Fig. 7a) and imaginary (χ''_{ac}) (not shown) components of the magnetic susceptibility and by the isothermal magnetization behavior at 2 K (Fig. 7b). Consistent with the increased separation between Ce centers and a more two-dimensional character of the magnetic lattice, the magnetic ordering temperatures in $CeSn_xSb_2$ are significantly lower than those in $CeSb_2$, for which $T_N \sim 15$ K (5).

Like $CeSb_2$, once long-range magnetic order is attained, the $CeSn_xSb_2$ series also undergoes field-induced magnetic transitions. At 2 K and an applied field of 1 T, $CeSn_{0.7}Sb_2$ and $CeSn_{0.5}Sb_2$ reach a saturation magnetization of ~1.4 μ_B/Ce (Fig. 7b), similar to that in $CeSb_2$ (1.1 μ_B/Ce at $H > 2$ T) (5). These values are considerably lower than 2.14 μ_B, expected for a $g_J = 6/7$ and $J = 5/2$ system. The lower saturation magnetization is attributed to CEF (crystalline electric field), lifting the degeneracy of the $J = 5/2$ ground term. An interesting characteristic of the magnetization loops of $CeSn_xSb_2$ is that the magnetization increases rapidly at low fields ($H < 0.1$ T) followed by a slower linear change ($0.1 < H < 1$ T) before saturating ($H > 1$ T). The coercivities are 4.6 Oe for $CeSn_{0.7}Sb_2$ and 12.6 Oe for $CeSn_{0.5}Sb_2$. $CeSb_2$ undergoes metamagnetic transitions at slightly higher fields (5). The evolution to a fan-type ferromagnetic structure suggested in $CeSb_2$ may equally be occurring in $CeSn_xSb_2$, but this needs to be verified by neutron diffraction experiments.

$PrSn_xSb_2$. The room-temperature effective moments are 3.73 μ_B/Pr for $PrSn_{0.7}Sb_2$ and 3.52 μ_B/Pr for $PrSn_{0.5}Sb_2$, which are close to that obtained for $PrSb_2$ (3.55 μ_B) (5). Analysis of the high temperature magnetic susceptibility data (Fig. 8a) leads to $\theta = -26$ K for $PrSn_{0.7}Sb_2$ and −27 K for $PrSn_{0.5}Sb_2$. This suggests that, at high temperatures,

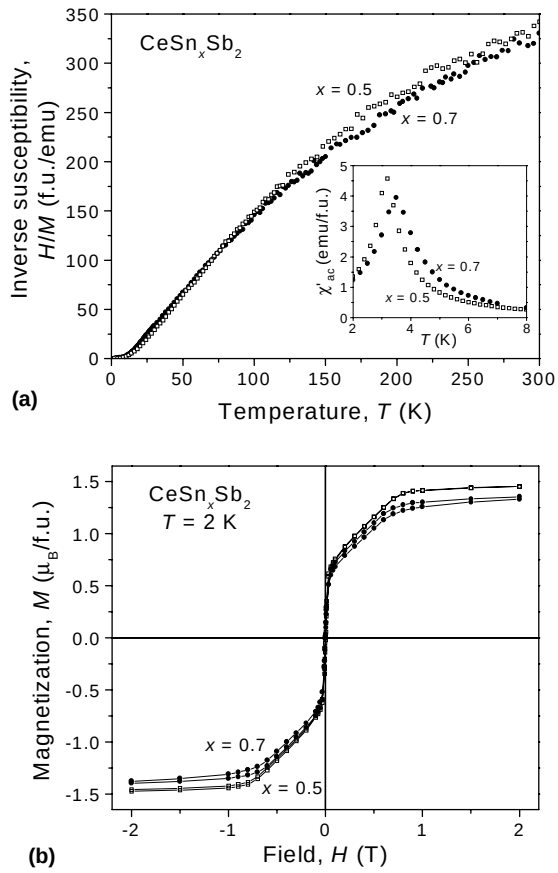

FIG. 7. Magnetic behavior of $CeSn_{0.7}Sb_2$ (filled symbols) and $CeSb_{0.5}Sb_2$ (open symbols). (a) Inverse magnetic susceptibility (H/M) with an applied field of 0.1 T between 2 and 300 K. Inset shows the low-temperature behavior of the ac magnetic susceptibility (χ'_{ac}) for $CeSn_{0.7}Sb_2$. (b) Isothermal magnetization at 2 K. Lines are included to guide the eye.

there are antiferromagnetic interactions occurring. The absence of a maximum in the magnetic susceptibility (M/H) curve above 2 K (inset Fig. 8a), the form of the isothermal magnetization curve at 2 K (Fig. 8b), and the absence of transitions in the resistivity curve (Fig. 5c) imply that long-range magnetic order is not attained in $PrSn_xSb_2$. This is in contrast to $PrSb_2$, which orders antiferromagnetically below 5.1 K and displays highly anisotropic isothermal magnetization and magnetoresistance behavior (5).

$NdSn_xSb_2$. The inverse magnetic susceptibilities (H/M) for $NdSn_{0.7}Sb_2$ and $NdSn_{0.5}Sb_2$ are shown in Fig. 9a. The paramagnetic Curie–Weiss temperatures are negative, with $\theta = -28$ K for $NdSn_{0.7}Sb_2$ and -14 K for $NdSn_{0.5}Sb_2$. The antiferromagnetic ordering temperature for $NdSn_{0.7}Sb_2$ ($T_N = 3.8$ K) coincides with the point at which a transition in the resistivity curve is observed, with $NdSn_{0.5}Sb_2$ magnetically ordering at 4.0 K. The ordering temperatures of these two compounds were determined from the χ'_{ac} susceptibility measurements shown in the inset of Fig. 9a. As was observed for $CeSb_2$ vs $CeSn_xSb_2$, the ordering temperature decreases significantly upon going from $NdSb_2$ ($T_N = 8$ K) (5) to $NdSn_{0.5}Sb_2$ (4.0 K) and then only slightly upon going to $NdSn_{0.7}Sb_2$ (3.8 K). This trend correlates with the expansion of the structure as more Sn is inserted between the $^2_\infty[RESb_2]$ layers.

$NdSb_2$ has been shown to undergo several extremely anisotropic metamagnetic transitions (5). Likewise, although measurements could only be performed on ground polycrystalline samples, the isothermal magnetization curves of both $NdSn_{0.7}Sb_2$ and $NdSn_{0.5}Sb_2$ at 2 K reveal a metamagnetic transition at $H_C = 5.5$ T followed by an approach to saturation at high fields with $M_{9T} = 1.7\,\mu_B$/Nd (Fig. 9b). When the results of several isotropic magnetization measurements are consolidated, the magnetic phase diagram for $NdSn_{0.7}Sb_2$ at low temperatures is obtained, showing the conditions under which the antiferromagnetic state occurs (Fig. 9c).

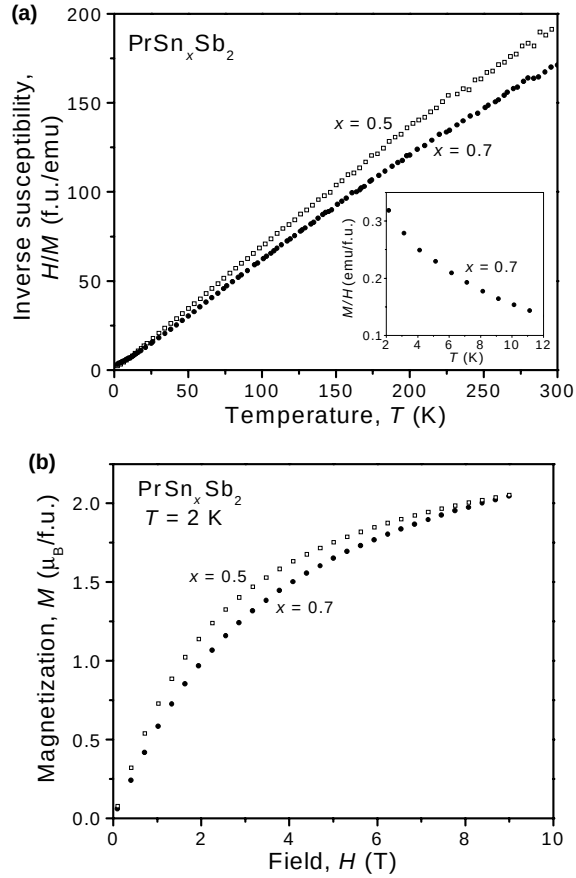

FIG. 8. Magnetic behavior of $PrSn_{0.7}Sb_2$ (filled symbols) and $PrSb_{0.5}Sb_2$ (open symbols). (a) Inverse magnetic susceptibility (H/M) with an applied field of 0.1 T between 2 and 300 K. Inset shows the low-temperature behavior of the magnetic susceptibility (M/H) for $PrSn_{0.7}Sb_2$. (b) Isothermal magnetization at 2 K.

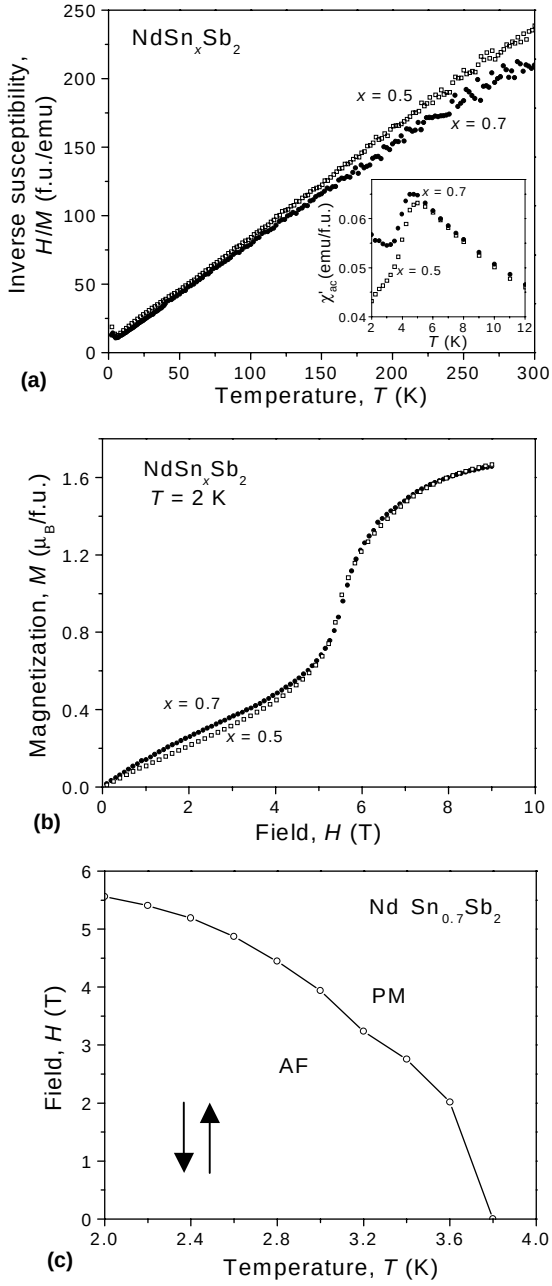

FIG. 9. Magnetic behavior of $NdSn_{0.7}Sb_2$ (filled symbols) and $NdSb_{0.5}Sb_2$ (open symbols). (a) Inverse magnetic susceptibility (H/M) with an applied field of 0.1 T between 2 and 300 K. Inset shows the low-temperature behavior of the ac magnetic susceptibility (χ'_{ac}) for $NdSn_{0.7}Sb_2$ and $NdSb_{0.5}Sb_2$. (b) Isothermal magnetization at 2 K. (c) Magnetic phase diagram delineating the $NdSn_{0.7}Sb_2$ antiferromagnetic and paramagnetic regimes.

$SmSn_xSb_2$. The temperature dependence of the susceptibility for both $SmSn_{0.7}Sb_2$ and $SmSn_{0.5}Sb_2$ shows that they do not display Curie–Weiss behavior (Fig. 10). The effective moments at 300 K are 1.57 μ_B/Sm for $SmSn_{0.7}Sb_2$ and 1.51 μ_B/Sm for $SmSn_{0.5}Sb_2$, which are comparable to

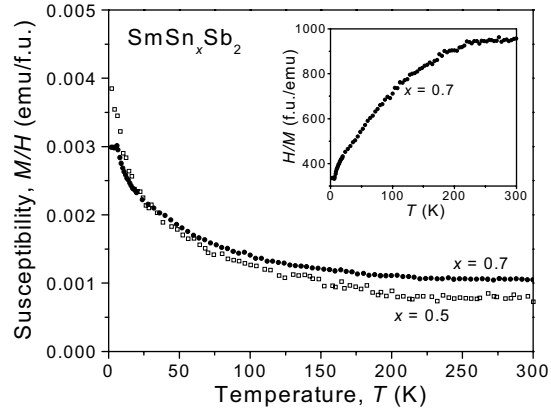

FIG. 10. Magnetic susceptibility (M/H) of $SmSn_{0.7}Sb_2$ (filled symbols) and $SmSn_{0.5}Sb_2$ (open symbols) between 2 and 300 K with an applied field of 0.5 T. Inset shows the temperature dependence of the inverse magnetic susceptibility (H/M) for $SmSn_{0.7}Sb_2$.

that observed for Sm-containing intermetallic compounds (13). Although the binary $SmSb_2$ displays long-range ordering at $T_N = 12.5$ K (6), the ternary $SmSn_xSb_2$ compounds do not display long-range magnetic ordering above 2 K. This absence of magnetic ordering is also reflected by the weak monotonic decrease in resistivity in this temperature range (Fig. 5c).

In summary, of the $RESn_xSb_2$ ($x = 0.5$, 0.7) series, long-range magnetic ordering above 2 K is observed for $CeSn_xSb_2$ (ferromagnetic below 3.5 K) and $NdSn_xSb_2$ (antiferromagnetic below 4.0 K). In general, the expansion of the structure as chains of zero-valent Sn atoms are inserted between $^2_\infty[RESb_2]$ layers reduces the magnetic interactions between the *RE* centers, as reflected by the lower transition temperatures for magnetic ordering to occur.

ACKNOWLEDGMENTS

The Natural Sciences and Engineering Research Council of Canada and the University of Alberta supported this work. We thank Dr. Robert McDonald (Faculty Service Officer, X-ray Crystallography Laboratory) for the data collection and Christina Barker for assistance with the EDX analysis.

REFERENCES

1. M. J. Ferguson, R. W. Hushagen, and A. Mar, *Inorg. Chem.* **35,** 4505 (1996).
2. R. Wang and H. Steinfink, *Inorg. Chem.* **6,** 1685 (1967).
3. N. L. Eatough and H. T. Hall, *Inorg. Chem.* **8,** 1439 (1969).
4. F. Hulliger and H. R. Ott, *J. Less-Common Met.* **55,** 103 (1997).
5. S. L. Bud'ko, P. C. Canfield, C. H. Mielke, and A. H. Lacerda, *Phys. Rev. B* **57,** 13624 (1998).
6. P. C. Canfield, J. D. Thompson, and Z. Fisk, *J. Appl. Phys.* **70,** 5992 (1991).

7. G. Oomi, T. Kagayama, K. Kawaguchi, P. C. Canfield, and S. L. Bud'ko, *Physica B* **230–232,** 776 (1997).
8. G. A. Papoian and R. Hoffmann, *Angew. Chem. Int. Ed.* **39,** 2408 (2000).
9. G. A. Papoian and R. Hoffmann, *J. Solid State Chem.* **139,** 8 (1998).
10. A. M. Mills and A. Mar, *J. Am. Chem. Soc.* **123,** 1151 (2001).
11. N. N. Greenwood and T. C. Gibb, "Mössbauer Spectroscopy." Chapman and Hall, London, 1971.
12. S. Kagoshima, H. Nagasawa, and T. Sambongi, "One-Dimensional Conductors." Springer-Verlag, Berlin, 1988.
13. A. Szytuła and J. Leciejewicz, Eds., "Handbook of Crystal Structures and Magnetic Properties of Rare Earth Intermetallics." CRC Press, Boca Raton, FL, 1994.